Journal of Power Sources 251 (2014) 145–151

Contents lists available at ScienceDirect

Journal of Power Sources

journal homepage: www.elsevier.com/locate/jpowsour

A dual-structured anode/Ni-mesh current collector hollow fibre for micro-tubular solid oxide fuel cells (SOFCs)

Tao Li, Zhentao Wu, K. Li*

Department of Chemical Engineering, Imperial College London, London SW7 2AZ, UK

HIGHLIGHTS

- Unique dual-structured ceramic hollow fibres are fabricated via a single-step technique.
- A mesh-structured inner Ni layer leads to low fuel transport resistance and efficient current collection.
- Finger-like micro-channels provide negligible fuel diffusional resistances.
- Excellent bulk electrical conductivity is obtained.
- Mechanical strength is suitable for full micro-tubular SOFCs and stacks.

ARTICLE INFO

Article history:
Received 19 August 2013
Received in revised form
21 October 2013
Accepted 9 November 2013
Available online 28 November 2013

Keywords:
Co-extrusion/co-sintering
Anodic current collector
Mesh structure
Micro-tubular SOFC

ABSTRACT

In this study, a unique dual-structured hollow fibre design has been developed for micro-tubular solid oxide fuel cells (MT-SOFCs), using a single-step phase-inversion assisted co-extrusion technique. The dual-structured design consists of an outer anode layer and an inner anodic current collecting layer that are formed simultaneously during fabrication. Meanwhile, a plurality of micro-channels initiating from the exterior surface of the anode layer penetrate through the two layers, forming a highly asymmetric anode and a mesh current collecting layer, which significantly facilitates the gas transport. With the increasing thickness of the current collecting layer (approximately 15–60 μm), electrical conductivity increases from 1.9×10^4 S cm^{-1} to 4.0×10^4 S cm^{-1}, while the mechanical strength drops slightly from approximately 168–113 MPa due to its 'dragging effect' during co-sintering. The benefits of improved current collection may potentially overweigh the reduced mechanical property, especially when dual-structured hollow fibres of this type are bundled together to form a stack. Moreover, benefiting from this innovative design, sustainable development of a larger scale of MT-SOFC stack or system becomes less challenging, since technical issues, such as concentration polarization and efficient current collection, hampering the MT-SOFC system design, can be completely overcome.

1. Introduction

A solid oxide fuel cell (SOFC) is a complete solid state device which electrochemically converts chemical energy from fuels to electric power without an intermediate combustion step. It has also been considered as one of the most promising technologies for sustainable energy generation due to its high efficiencies (>60%) and low or zero emission of pollutants (SO_2 and NO_x) [1–3]. In addition, the high-grade exhaust heat could be utilized to drive gas turbines or be stored in a medium, so the overall system efficiency could be further increased to more than 80%. As a result, planar SOFCs, which have received probably the most interest due to its simple cell geometry and good fabricability, have been successfully commercialized, such as domestic combined heat and power (CHP) system and auxiliary power units (APUs) [2,4].

The micro-tubular geometric design with rapid start-up/shut-down, high power density, good cycling performance and thermal shock resistance [5] has started to attract research attentions since early 1990s. However, its development is still at R&D phase due to several technical challenges, such as the complexity in fabrication processes that limit mass-scale production and the difficulties in economically and efficiently collecting current from electrodes, especially from the small lumen of micro-tubes.

In terms of fabricating micro-tubular SOFCs, co-extrusion technique [6–8] considerably simplifies the fabrication process by forming a number of layers simultaneously, together with other

* Corresponding author. Tel.: +44 207 5945676; fax: +44 207 5945629.
E-mail address: Kang.Li@imperial.ac.uk (K. Li).

0378-7753/$ – see front matter © 2013 Elsevier B.V. All rights reserved.
http://dx.doi.org/10.1016/j.jpowsour.2013.11.043

advantages such as great process control, adjustable morphologies and reduced fabrication costs. Moreover, this technique allows a stronger adhesion between cell components, leading to less ohmic loss and over-potential resistance. This is a genuine technology breakthrough when compared with conventional fabrication techniques involving repeated coating and sintering steps. With regards to scale-up, how to economically and efficiently collect current, especially from the lumen side of each micro-tubular cell, without creating further mass transfer resistance is still a challenge, as it determines the overall performance of the corresponding MT-SOFC systems.

Most of MT-SOFCs are anode-supported, and various techniques have been reported for anodic current collection, such as inserting nickel mesh and pin into the anodic lumen [9], connecting one end of anode uncovered by electrolyte [10–12] and sintering gold or silver layers [13]. However, reproducibility and actual contact between anode and current collector need to be considered when evaluating the overall cell performance. Recently, Lee et al. [14] have developed a novel technique, in which the current collection is integrated with fuel supply by using a conductive fuel inlet pipe connected with nickel wires. A significantly increased power density (from 0.24 to 0.54 W cm^{-2}) and fuel utilization rate (45%) can thus be achieved, leading to a new combined system with lower ohmic losses and contact resistance between the anode and current collector. However, a more cost-effective and efficient current collection technique addressing good fabricability, great adhesion to anode, negligible gas transfer resistance and suitable for scaling-up is still of great interest.

This study is based on one of our previous researches [15], in which the feasibility of using a phase-inversion assisted co-extrusion technique to fabricate Ni–YSZ (yttria-stabilized zirconia, anode)/Ni (anodic current collector) dual-layer hollow fibres has been proved. Besides different materials and adjustable layer thicknesses, more benefits in designing micro-structures [7,16], such as a highly asymmetric anode and mesh current collector, for potentially less mass transfer resistance inside anode and between the two layers have been incorporated in this study. As a result, less concentration polarization inside anode and efficient anodic current collection generated may contribute to a more sustainable development of micro-tubular SOFC stacks and systems.

2. Experimental

2.1. Materials

Commercially available cerium-gadolinium oxide ($Ce_{0.9}Gd_{0.1}O_{1.95}$ (CGO), surface area 35.6 m^2 g^{-1}, mean particle size (d50) 0.1–0.4 μm, NexTech Materials Ltd., USA) and nickel oxide (NiO, surface area 3.7 m^2 g^{-1}, mean particle size (d50) 12–22 μm, NexTech Materials Ltd., USA) were used as supplied. Polyethersulfone (PESf) purchased from Radel A-300, Ameco Performance (USA), and dimethyl sulfoxide (DMSO) purchased from VWR International, LLC were used as the polymer binder and the solvent, respectively. Polyethyleneglycol 30-dipolyhydroxystearate (Arlacel P135, Uniqema) was used as the dispersant of the spinning suspension. During the co-extrusion, DMSO and tap water were the internal and external coagulants, respectively.

2.2. Fabrication of anode/anodic current collector dual-structured hollow fibres

Spinning suspensions of anode and anodic current collector were prepared separately, with the detailed compositions listed in Table 1. Typically, Arlancel P135 was dissolved in solvent (DMSO) prior to the addition of ceramic powders, and the mixture was milled for 2–3 days (JARMILL, Gladstone Engineering. LTD, UK). The mixing was further conducted for another 3–4 days after adding the organic binder (10 wt% of ceramic powders) to obtain homogeneous spinning suspensions. Before being transferred into stainless steel syringes, both spinning suspensions were degassed under vacuum with stirring in order to eliminate air bubbles inside. The dual-layer precursors were fabricated by a phase-inversion assisted co-extrusion technique described elsewhere [17]. Pure solvent (DMSO) was adopted as the internal coagulant to obtain the mesh current collector. The extrusion rates of internal coagulant and two suspensions were accurately controlled by syringe pumps (Harvard PHD22/200 HPsi and KDS410). The extrusion rates of internal coagulant and anode were maintained at 6 and 7 ml min^{-1}, respectively, while the extrusion rate of inner current collecting layer was reduced from 2 to 0 ml min^{-1} for tailoring the thickness. Precursor fibres were left in the external coagulant bath overnight to complete the solidification of polymer binder, before being cut to a length of 15 cm.

Table 1
Compositions of the spinning suspensions for dual-structured hollow fibres.

Materials	Anode (wt.%)	Current collector (wt.%)
NiO	40.1	69.6
CGO	26.8	/
Polymer binder (PESf)	6.69	6.96
Dispersant (Arlacel P135)	0.15	0.15
Solvent (DMSO)	26.2	23.3

The co-sintering was undertaken in static air to yield dual-structured ceramic hollow fibres using a tubular furnace (CARBOLITE). The temperature was first increased to 400 °C at a rate of 2 °C min^{-1} and held for 1 h, then to 800 °C at a rate of 2 °C min^{-1} and held for 2 h, and finally to 1500 °C at a rate of 15 °C min^{-1} and held for 12 h. The temperature was then decreased to room temperature at the rate of 3 °C min^{-1}. For post-sintering characterizations, the co-sintered hollow fibres need to be reduced, converting NiO into Ni. The reduction was conducted in a pure hydrogen atmosphere by packing fibres into a stainless steel tube placed in a CARBOLITE furnace (MTF 12/25/250). Initially, argon (~30 ml min^{-1}, 25 °C, 1 atm) was used to expel air inside the tube, until the furnace temperature reached 550 °C (heating rate of 5 °C min^{-1}). Then the argon flow was changed to a pure hydrogen flow (~20 ml min^{-1}, 25 °C, 1 atm) and the reduction lasted for 2 h. After the reduction, the hydrogen flow was changed back to argon flow until the furnace temperature was reduced to room temperature at a rate of 5 °C min^{-1}.

2.3. Characterizations

Prior to the co-sintering, shrinking behaviours of both anode and current collector materials were studied using a dilatometer (NETZSCH, model DIL 402C). Powder mixtures were compressed into bars of 6 mm × 6 mm × 6 mm by using a custom-designed mould. The measurements were carried out in static air and the system was heated up to 1500 °C at 5 °C min^{-1}.

The morphology of the dual-layer hollow fibres was investigated using scanning electron microscopy (SEM) characterization (JOEL JSM-5610). Samples were gold-coated under vacuum for 1.5 min at 20 mA (EMITECH Model K550) and SEM images with different magnification were collected under both secondary electrons imaging (SEI) and backscattered electrons (BSE) modes. Energy dispersive spectrometry (EDS, JEOL JSM-6400 electron microscope) analyses was also undertaken to investigate the elemental distribution inside the fibres.

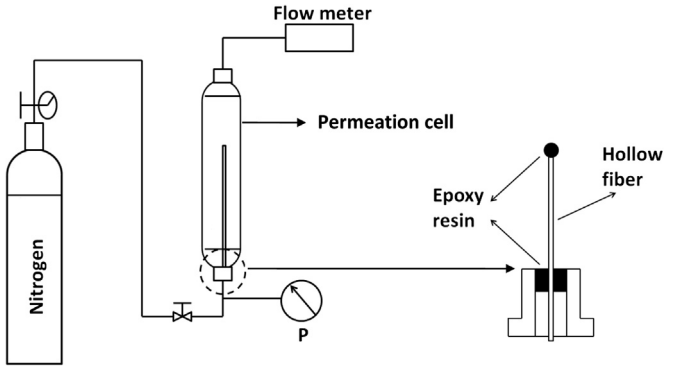

Fig. 1. Schematic diagram of the set-up for gas-permeation test.

The average porosity was studied using a pycnometer (Micromeritics Accupyc 1330) via Archimedes method. The skeleton density of the hollow fibres ρ_{pyc} (g cm^{-3}) was first determined by changing pressures of helium in a calibrated volume. The average porosity (ε_V) was then calculated using the equations below:

$$\varepsilon_V = \frac{\rho_{pyc} - \rho_{fibre}}{\rho_{pyc}} \quad (1)$$

$$\rho_{fibre} = \frac{4m_{sample}}{\pi\left(D_o^2 - D_i^2\right)l_{sample}} \quad (2)$$

where m, l, D_o and D_i represent the mass (g), length, outer and inner diameters of the sample (cm), respectively.

Mechanical strength was studied by a three-point bending method using a tensile tester (Instron Model 5544) with a load cell of 5 kN. Samples were cut to a certain length ($\sim$50 mm) and placed on two sample holders which had a gap of 30 mm. The fracture force was obtained and the bending strength was then calculated using the following equation:

$$\sigma_F = \frac{8FLD_o}{\pi\left(D_o^4 - D_i^4\right)} \quad (3)$$

where F denotes the measured fracture force (N), L, D_o and D_i represent the length (m), the outer and inner diameters of the fibre (m), respectively.

Gas permeability was investigated using N_2 permeation method at room temperature, details of which have been described elsewhere [18]. Hollow fibre samples were sealed into the system using epoxy resin and the feed pressures were adjusted using a pressure regulator, as illustrated in Fig. 1. The flow rate of N_2 was measured using a bubble flow meter and the gas permeance was then calculated using the equation below:

$$P = \frac{Q \cdot \ln(D_o/D_i)}{\pi L(D_o - D_i)\cdot\Delta p} \quad (4)$$

where P denotes the permeance of N_2 (mol m^{-2} s^{-2} Pa^{-1}), L, D_o and D_i represent fibre length (m), the outer and inner diameters of the fibre (m), respectively, and ΔP is the pressure difference across the hollow fibre (Pa).

The electrical conductivity of the dual-layer hollow fibre was measured using a four-point direct current method at room temperature, details of which can be found elsewhere [16]. Silver wires were inserted into both ends for a depth of $\sim$5 mm and attached to the lumen using silver paste. Samples were subsequently connected in the circuit. Voltage drop across the samples of 50 mm were obtained using a multimeter by passing controlled currents (50 mA, 75 mA and 100 mA). Bulk conductivity (σ_{fibre}, S cm^{-1}) of the

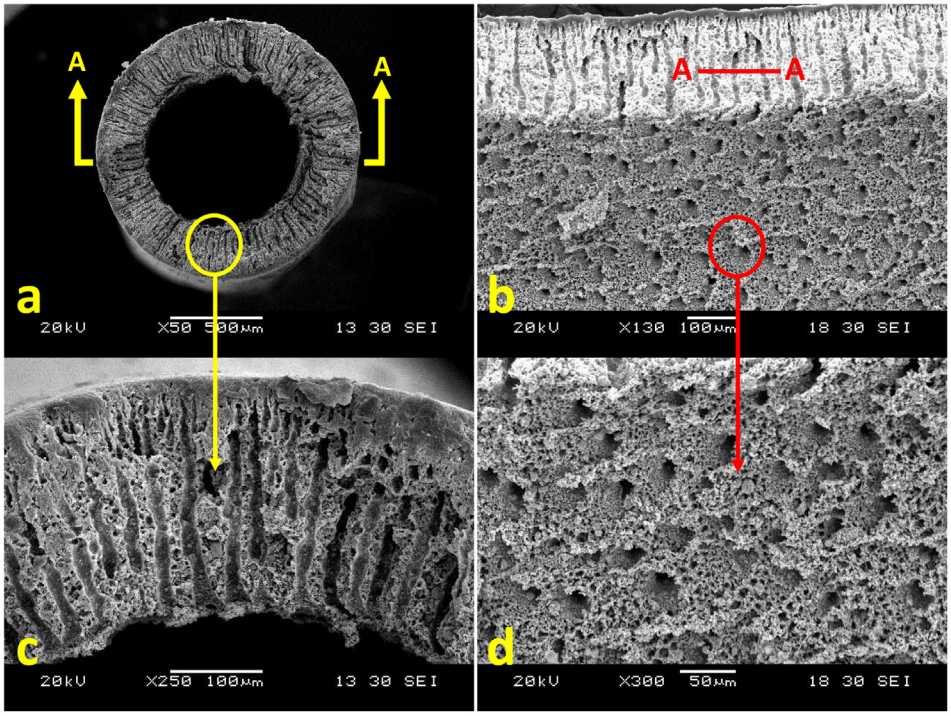

Fig. 2. SEM images (secondary electron imaging (SEI) mode) of the dual-layer precursor fibre with the current collector extrusion rate of 2 ml min^{-1}: (a) and (c) cross section in radial direction, (b) cross section in axial direction, (d) inner surface.

dual-structured hollow fibres was then estimated using the equation below:

$$\sigma_{\text{fibre}} = \frac{L_{\text{fibre}}}{A_{\text{fibre}} \times R_{\text{fibre}}} \quad (5)$$

where A_{fibre} represents the cross-sectional area (cm^2), $A_{\text{fibre}} = \pi/4(D_o^2 - D_i^2)$; L_{fibre} is the fibre length (50 mm); $R_{\text{resistance}}$ denotes the fibre resistance calculated based on the linear fits of obtained I–V data.

3. Results and discussion

3.1. Morphology of dual-structured hollow fibres

Fig. 2 presents the cross-sectional morphologies of a selected precursor fibre. Finger-like micro-channels originating from the outer surface have penetrated through the entire cross section (Fig. 2(a) and (c)), which is a result of zero air gap and using solvent as the internal coagulant. It has been generally accepted that the formation of the finger-like micro-channels is resulted from hydrodynamically unstable viscous fingering phenomenon [19], which takes place at the interface between two fluids of different viscosities at the first moment of mixing. When the spinning suspension is in contact with non-solvent (H_2O), the solvent/non-solvent exchange leads to the increase in dynamic viscosity of suspension and the precipitation of the polymer phase. However, there exists a critical viscosity threshold above which the formation of finger-like micro-channels is completely suppressed despite the non-solvent influx; in other words, viscous fingering only occurs when the initial viscosity of spinning suspensions is below the threshold and the growth of micro-channels will be halted once the dynamic viscosity is above the threshold. By using solvent (DMSO) as the internal coagulant, the dynamic viscosity of suspensions at the front of finger-like micro-channels is maintained at a value below the threshold, so the growth of the finger-like micro-channels can continue until penetrating through the entire cross section of the fibre, giving the mesh structure on the inner surface, as shown in Fig. 2(b) and (d). The holes on the inner surface were estimated at around 20 μm in precursor fibres.

Fig. 3 illustrates the SEM images of the co-sintered dual-structured hollow fibre. The finger-like micro-channels were well preserved during the sintering (Fig. 3(a) and (b)) and the holes on the inner surface were reduced to around 10 μm (Fig. 3(c) and (d)). Meanwhile, the two layers could be clearly distinguished (Fig. 3(b)), due to the remove of polymer binder in precursor counterpart. The darker layer denotes the inner current collecting layer, while the lighter layer is anode. After reducing NiO into Ni, the mesh-like

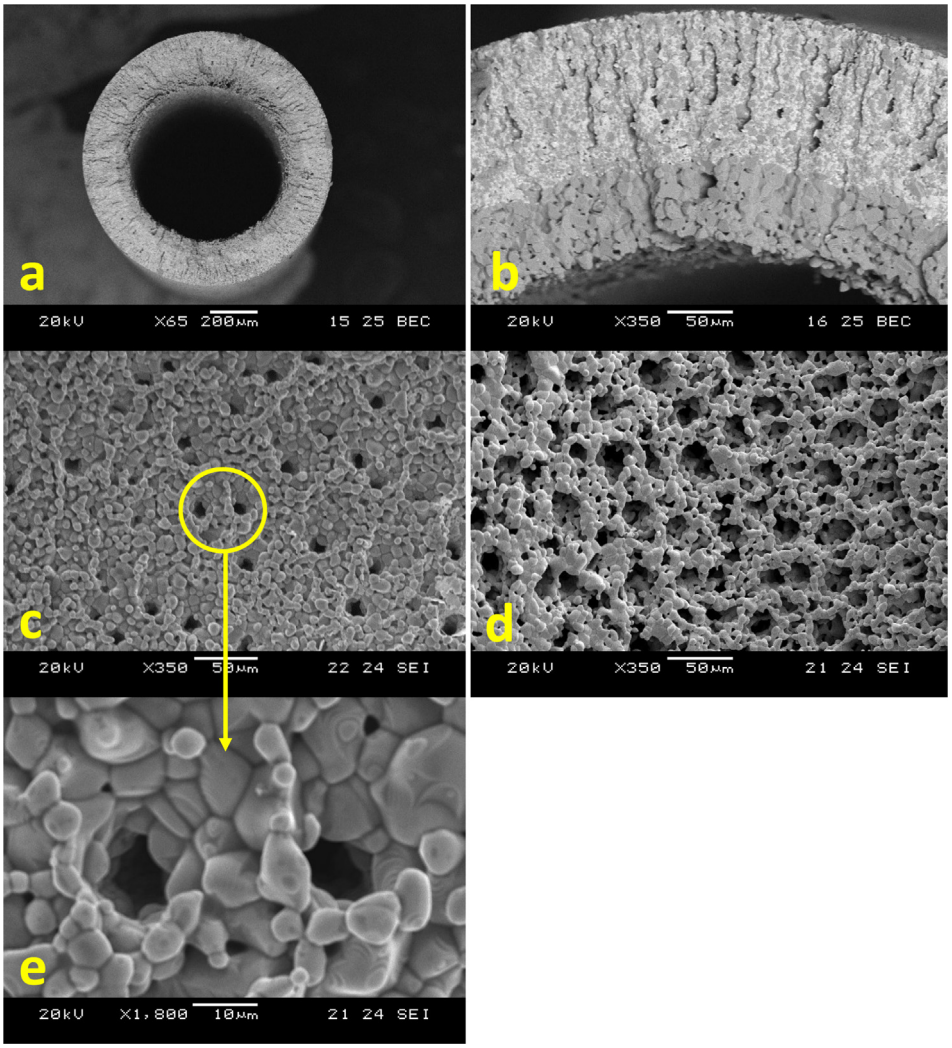

Fig. 3. SEM images of sintered dual-layer fibre with the current collector extrusion rate of 2 ml min^{-1}: (a, b) cross-section (c, e) inner surface; (d) inner surface of reduced fibre.

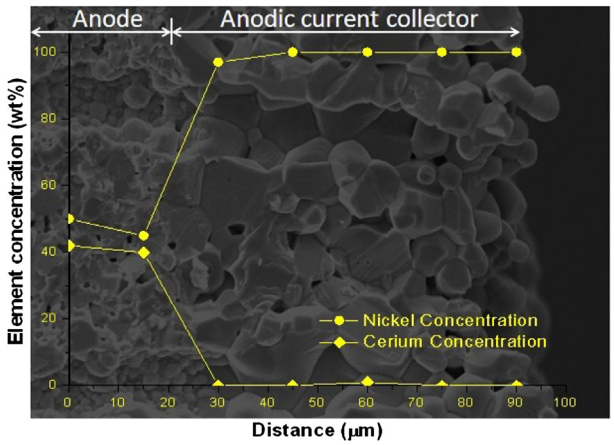

Fig. 4. EDS results of interface between the inner current collector (right side) and outer anode layer (left side).

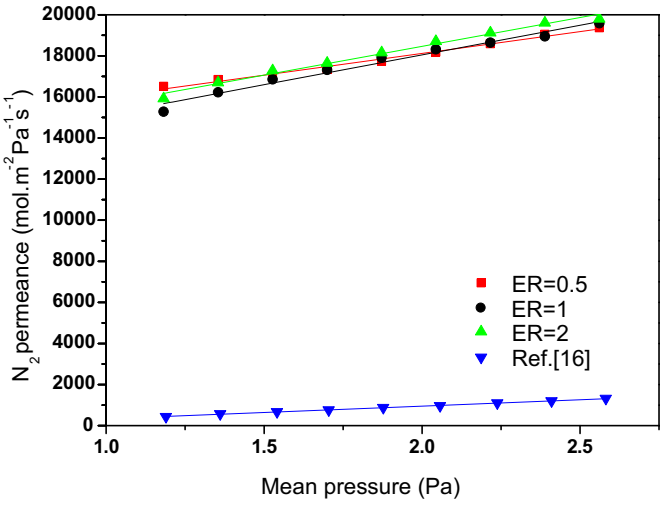

Fig. 5. The N_2 permeation results of anode/anodic current collector dual-structured hollow fibre (ER represents the extrusion rates of anodic current collector during co-extrusion).

structure in the current collecting layer is more significant (Fig. 3(e)). The inter-layer diffusion during cell fabrication needs to be minimized, since it reduces cell efficiency [6]. EDS analysis shown in Fig. 4 proves that no observable inter-layer diffusion can be found at the interface between anode and current collector. While due to the fact that NiO exist in both anode and current collecting layer and the two layers are co-extruded and co-sintered simultaneously, great adhesion can thus be formed.

Detailed dimensions of the dual-structured hollow fibres fabricated at controlled inner layer extrusion rates (0, 0.5, 1 and 2 ml min^{-1}) are listed in Table 2. The thickness of the inner current collecting layer increases from approximately 15–60 μm when the extrusion rate is increased from 0.5 to 2 ml min^{-1}. Meanwhile, outer diameter of the fabricated fibres is maintained at a nearly constant value, due to the instant precipitation of the polymer binder at the outer surface when it is in contact with the excessive external coagulant (zero air gap).

3.2. Gas diffusion inside the dual-structured hollow fibres

Li et al. [20] studied the theoretical effects of membrane pore structure parameters, such as pore size, pore size distribution and effective surface porosity, on the membrane's coefficient. They concluded that when the pore radius is greater than 1 μm, membrane's coefficient is governed solely by the continuum diffusion coefficient. Since the "pores" in our inner current collecting layer are around 10 μm, fuel diffusion resistance across this layer is negligible.

Fig. 5 shows the experimental results of gas permeation. The gas permeance test was conducted using N_2 at room temperature to determine the gas transport behaviour. As can be seen, samples with different current collector extrusion rates display very similar gas permeation behaviour, indicating that the thickness of anodic current collect has a negligible influence on gas permeation. This agrees well with the conclusion of Li et al. [20] and indicates that the resistance of fuel diffusion through the mesh current collecting layer is negligible. When compared with previous research [16], the N_2 permeability obtained in this study is around 10 times higher, which is probably due to the considerable decrease in the thickness of sponge-layer in this study.

In addition to that, micro-channels (well wider that 2 μm) inside the anode layer play an important role in affecting fuel, normally H_2, diffusion pathways and distribution. One of our previous studies [1,16] has proved that the finger-like micro-channels inside anode layer significantly reduced mass transfer related concentration polarization. This is also considered as one of the major reasons for the high cell performance achieved (2.3W cm^{-2} at 600 °C) [1]. This advantage has been incorporated into the dual-structured hollow fibre design in this study, and its effects on H_2 diffusion pathways and distribution are schematically presented in Fig. 6, and compared with our previous anode/current collector design [15].

The beneficial effect of the long finger-like micro-channels results in that H_2 not only can diffuse easily into the anode layer, but also distribute evenly inside the anode of this type. This contributes to a possibly much lower mass transfer related concentration polarization when compared with our previous design, in which H_2 needs to diffuse through a nearly full sponge-like structure with an average pore size of 0.3 μm. Reactive sites are thus more accessible to H_2 due to a shorter and less tortuous pathway. For conventional symmetric anode, there exists a trade-off between a large quantity of accessible reactive sites and a low fuel transport resistance. Porosity is one of the parameters to evaluate the balance of the two factors. Dong et al. [21] has suggested an ideal anode porosity ranging from 30% to 40% based on a seepage theory. The average

Table 2
Dimensions and porosity of dual-structured hollow fibres.

Extrusion rate of current collector (ml min^{-1})	OD (μm)	ID (μm)	Thickness of current collector (μm)	Thickness of anode (μm)	Current collector/overall thickness (%)	Average porosity (%)
0	1069.8	693.0	/	189.5	/	32.2
0.5	1064.9	679.6	15.2	177.5	7.9	34.7
1	1066.3	658.9	28.3	175.3	13.9	36.3
2	1068.9	633.0	59.9	158.0	27.5	40.6

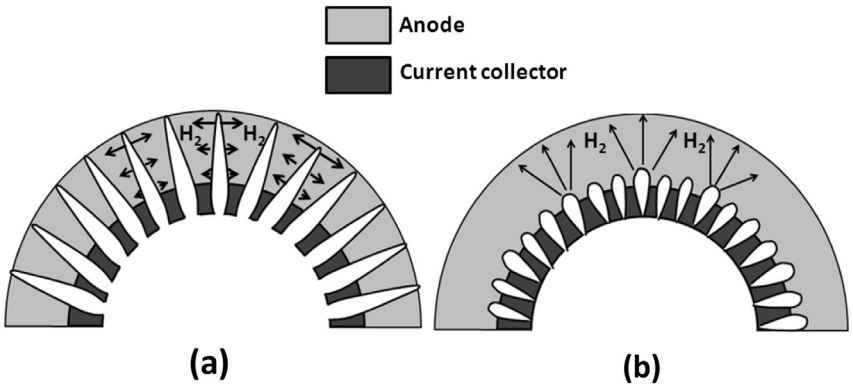

Fig. 6. Illustration of the H_2 diffusion pathway in the anode/anodic current collector dual-layer hollow fibre. (a) Hollow fibre with long finger-like voids from outer surface in this study; (b) Hollow fibre with short finger-like voids in Ref. [15].

porosity of the dual-structured hollow fibre in this study (Table 2) increases with the current collector thickness and locates well within the suggested porosity. Moreover, the substantially decreased mass transfer resistance would benefit further in the development of larger stacks with higher system efficiencies.

3.3. Mechanical property

Mechanical strength is one of the essential aspects that determine the life of fuel cells. For the dual-structured hollow fibre, both fracture force and bending strength decrease when the thickness of current collector is increased (Fig. 7). This is due to the reduced anode thickness as shown in Table 2, which is the main provider of the mechanical strength, and excessive shrinking behaviour of the inner layer. As can be seen in Fig. 8(a), NiO (inner layer material) starts to shrink at a lower temperature, and finishes at a higher shrinkage when compared with the anode material (60%NiO–40% CGO). Meanwhile, the maximum sintering rate of NiO is higher and turns up at a lower temperature (Fig. 8(b)). All these indicate that the inner layer keeps "dragging" the outer layer during the co-sintering, hindering the proper densification of anode layer and subsequently leads to reduced mechanical strength. And such a kind of dragging effect is more significant with a thicker current collecting layer. The maximum bending strength at the thinnest current collecting layer (15 μm) is approximately 168 MPa and is comparable with previous studies [15,16,22], in which asymmetric anode supported designs were fabricated via a similar method. In addition, Yang et al. [23] have suggested that, for an anode supported design, bending strength of around 150 MPa could be well applied for the construction of micro-tubular SOFCs. And when bundled together, mechanical strength of a micro-tubular stack can be significantly improved.

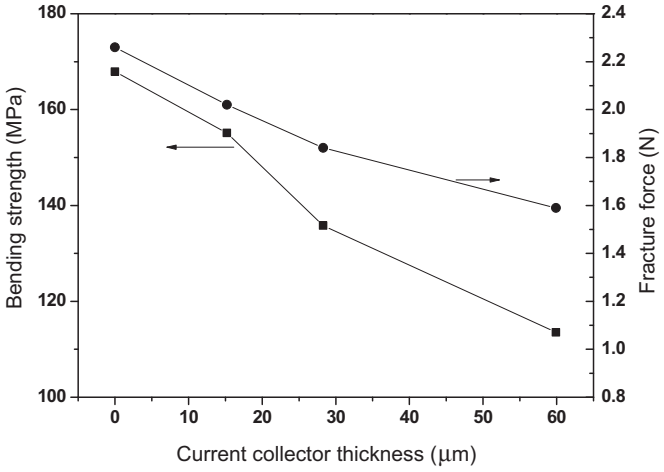

Fig. 7. Bending strength and fracture force as a function of different current collector thicknesses.

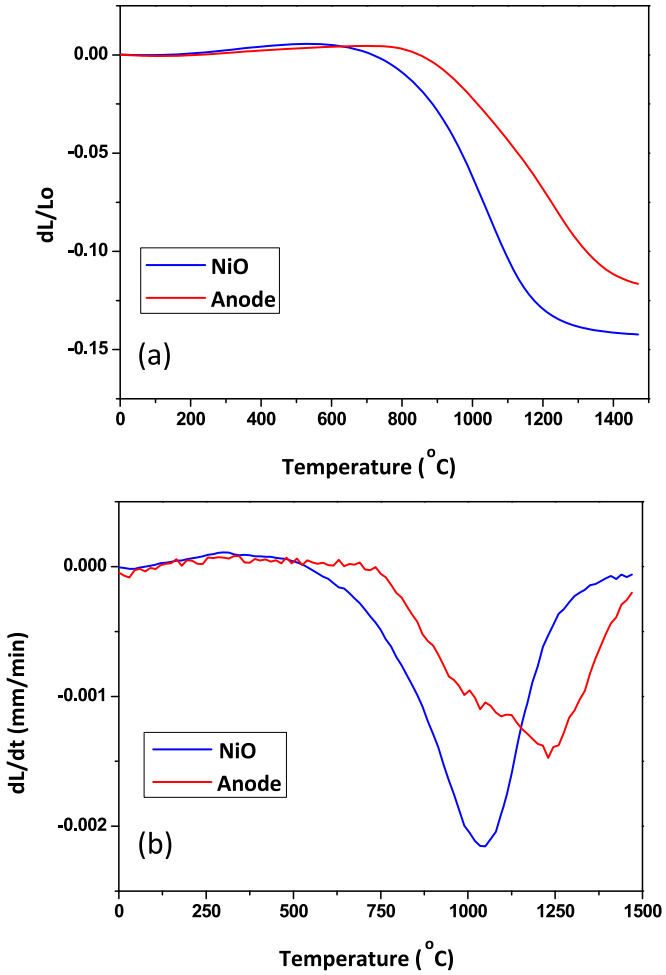

Fig. 8. (a) Sintering curves of NiO and the materials of anode (Heating rate: 5 °C min^{-1}); (b) Sintering rate curves of NiO and the materials of anode.

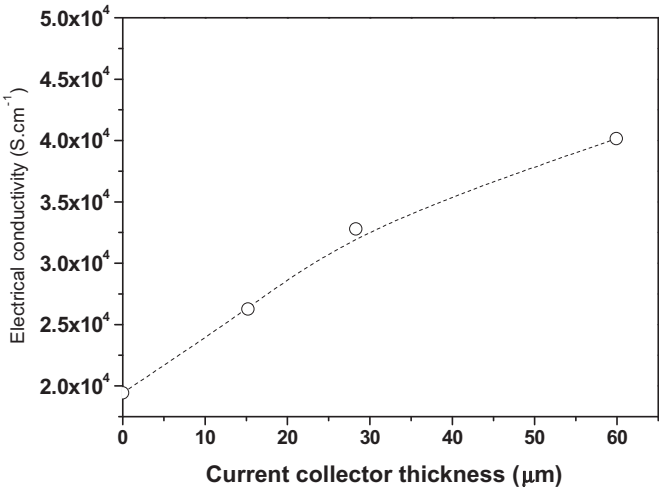

Fig. 9. Electrical conductivity of reduced anode/anodic current collector dual layer hollow fibres as a function of current collector thickness.

3.4. Electrical conductivity

In general, this study aims at developing an effective and sustainable way of collecting current from the lumen side of MT-SOFCs, and therefore, the electrical conductivities of the dual-structured hollow fibres are illustrated in Fig. 9. As can be seen from the figure, the conductivity of the single-layer counterpart (current collector extrusion rate is 0 ml min^{-1}) agrees quite well with other studies [6,16]. By adding an inner current collecting layer, the bulk conductivity is increased markedly. The conductivity of the sample with the thickest current collecting layer (4.1×10^4 S cm^{-1}) doubles the value of the single-layer counterparts, which proves the feasibility of using such design for further development of MT-SOFC stacks. However, it is still lower than our previous anode/current collector design (7.7×10^4 S cm^{-1}). This indicates that the long finger-like micro-channels facilitate fuel diffusion inside anode, while, in the mean time, reduces bulk conductivity.

By combining the advantages of long finger-like micro-channels inside anode [7] and efficient current collection, the dual-structured anode/anodic current collector design is suitable to be applied for the construction of a complete micro-tubular SOFC. Moreover, the simplified and reliable single-step fabrication process presented in this study is promising for mass-scale production and would contribute to further in the development of MT-SOFC stacks and systems.

4. Conclusions

A dual-structured Ni/Ni-CGO hollow fibre has been successfully fabricated via a phase-inversion assisted co-extrusion/wet-spinning technique. By applying solvent as internal coagulant, finger-like micro-channels originating from the outer surface have penetrated the whole cross-section resulted in a mesh structure with long micro-channels, which can substantially reduce the fuel transport resistance, as the long micro-channels inside anode provide more evenly distributed and easier pathways for H_2 diffusion. By adjusting the extrusion rates, precise control over the thickness of current collecting layer can be achieved with good adhesion between the two layers. Increasing the thickness of current collector leads to an increased average porosity and electrical conductivity, but a decreased mechanical strength. By combining the advantages of the reduced fuel mass transfer resistance and efficient current collection, such dual-structured hollow fibre design creates more possibilities for sustainable development of MC-SOFCs.

Acknowledgement

The authors gratefully acknowledge the research funding provided by EPSRC in the United Kingdom (Grant No. EP/G012679/1).

References

[1] N.Q. Minh, T. Takahashi, Science and Technology of Ceramic Fuel Cells, Elsevier Science, Oxford, UK, 1995.
[2] S.C. Singhal, K. Kendall, W. Winkler, in: S.C. Singhal, Hendall (Eds.), High Temperature Solid Oxide Fuel Cells: Fundamentals, Designs and Applications, Elsevier Oxford, UK, 2003.
[3] R.M. Ormerod, Chem. Soc. Rev. 32 (2003) 17–28.
[4] K.S. Weil, C.A. Coyle, J.S. Hardy, J.Y. Kim, G.-G. Xia, Fuel Cells Bull. 2004 (2004) 11–16.
[5] K. Kendall, Int. J. Appl. Ceram. Technol. 7 (2010) 1–9.
[6] M.H.D. Othman, Z. Wu, N. Droushiotis, U. Doraswami, G. Kelsall, K. Li, J. Membr. Sci. 351 (2010) 196–204.
[7] M.H.D. Othman, N. Droushiotis, Z. Wu, G. Kelsall, K. Li, Adv. Mater. 23 (2011) 2480–2483.
[8] M.H.D. Othman, N. Droushiotis, Z. Wu, K. Kanawka, G. Kelsall, K. Li, J. Membr. Sci. 365 (2010) 382–388.
[9] T.J. Lee, K. Kendall, J. Power Sources 181 (2008) 195–198.
[10] T. Suzuki, Y. Funahashi, Z. Hasan, T. Yamaguchi, Y. Fujishiro, M. Awano, Electrochem. Commun. 10 (2008) 1563–1566.
[11] T. Suzuki, T. Yamaguchi, Y. Fujishiro, M. Awano, J. Electrochem. Soc. 153 (2006) A925.
[12] T. Suzuki, T. Yamaguchi, Y. Fujishiro, M. Awano, J. Power Sources 160 (2006) 73–77.
[13] R. Zheng, H. Rho, L. Yamarte, G.J. Kovacik, P. Sarkar. Controlling Solid Oxide Fuel Cell Operation, Patent number US7258936, Alberta Research Council, Inc., United States, 2004.
[14] S.-B. Lee, T.-H. Lim, R.-H. Song, D.-R. Shin, S.-K. Dong, Int. J. Hydrogen Energy 33 (2008) 2330–2336.
[15] K. Kanawka, M.H.D. Othman, N. Droushiotis, Z. Wu, G. Kelsall, K. Li, Fuel Cells 11 (2011) 690–696.
[16] M.H.D. Othman, Z. Wu, N. Droushiotis, G. Kelsall, K. Li, J. Membr. Sci. 360 (2010) 410–417.
[17] B. Zydorczak, Z. Wu, K. Li, Chem. Eng. Sci. 64 (2009) 4383–4388.
[18] S. Liu, Ceram. Int. 29 (2003) 875–881.
[19] B.F.K. Kingsbury, K. Li, J. Membr. Sci. 328 (2009) 134–140.
[20] K. Li, J. Kong, X. Tan, Chem. Eng. Sci. 55 (2000) 5579–5588.
[21] D. Dong, J. Gao, X. Liu, G. Meng, J. Power Sources 165 (2007) 217–223.
[22] N. Yang, X. Tan, Z. Ma, J. Power Sources 183 (2008) 14–19.
[23] C. Yang, W. Li, S. Zhang, L. Bi, R. Peng, C. Chen, W. Liu, J. Power Sources 187 (2009) 90–92.